

REGULAR PAPER

Preparation of high-quality thick AlN layer on nanopatterned sapphire substrates with sputter-deposited annealed AlN film by hydride vapor-phase epitaxy

To cite this article: Shiyu Xiao *et al* 2019 *Jpn. J. Appl. Phys.* **58** SC1003

View the [article online](#) for updates and enhancements.

You may also like

- [Surface Planarization of GaN-on-Sapphire Template by Chemical Mechanical Polishing for Subsequent GaN Homoepitaxy](#)
Hideo Aida, Seong-woo Kim, Toshimasa Suzuki *et al.*
- [Period size effect induced crystalline quality improvement of AlN on a nano-patterned sapphire substrate](#)
Nan Xie, Fujun Xu, Na Zhang *et al.*
- [An ITER-relevant passive active multijunction launcher for lower hybrid current drive in JET-grade plasmas](#)
Jorge H. Belo, Philippe Bibet, João P.S. Bizarro *et al.*



Preparation of high-quality thick AlN layer on nanopatterned sapphire substrates with sputter-deposited annealed AlN film by hydride vapor-phase epitaxy

Shiyu Xiao^{1*}, Nan Jiang², Kanako Shojiki², Kenjiro Uesugi³, and Hideto Miyake^{1,2}

¹Graduate School of Regional Innovation Studies, Mie University, Mie 514-8507, Japan

²Graduate School of Engineering, Mie University, Mie 514-8507, Japan

³Organization for Promotion of Regional Innovation, Mie University, Mie 514-8507, Japan

*E-mail: xiao@innov.mie-u.ac.jp

Received December 31, 2018; accepted February 17, 2019; published online April 16, 2019

A crack-free aluminum nitride (AlN) layer of $9 \pm 1 \mu\text{m}$ thickness was grown on a nanopatterned sapphire substrate (NPSS) with a sputter-deposited AlN buffer layer. The buffer layer was thermally annealed and AlN was regrown by hydride vapor-phase epitaxy (HVPE). The dependence of the crystallinity of HVPE-grown AlN layers on the growth temperature was investigated. It was found that undesired misaligned AlN growth can be prevented by choosing an appropriate growth temperature. The full widths at half maximum of the (0002)- and (10–12)-plane X-ray rocking curves were improved to as low as 102 and 219 arcsec, respectively, by applying an NPSS with a sputter-deposited annealed AlN film. Compared with substrates without nanopatterning, the NPSS was also effective for suppressing cracks owing to the formation of voids at the interface of the HVPE-grown AlN layer and NPSS template. © 2019 The Japan Society of Applied Physics

1. Introduction

$\text{Al}_x\text{Ga}_{1-x}\text{N}$ -based optoelectronic devices such as UV-LEDs have attracted worldwide attention. A thick aluminum nitride (AlN) layer is commonly used as a crucial template between a sapphire substrate and AlGaN for deep UV-LEDs.^{1–10)} To realize the full potential of such devices, a high-quality AlN template is essential. Numerous groups have attempted to grow AlN crystals.^{11–16)} Hydride vapor-phase epitaxy (HVPE) is one of the promising approaches for the preparation of freestanding AlN substrates or thick templates because of its high growth rate and low carbon impurity incorporation.^{17–19)} Several groups have demonstrated the growth of AlN directly on sapphire substrates by HVPE. The best X-ray diffraction (XRD) rocking curve FWHM values were in the ranges of 120–600 arcsec for the (0002) reflection and above 400 arcsec for the (10–12) reflection.^{20–24)} Moreover, it is still challenging to grow a crack-free thick AlN layer with high crystallinity on a flat sapphire substrate (FSS) owing to the large difference in the thermal expansion coefficients and lattice constants between AlN and the sapphire substrate. Nanopatterned sapphire substrates (NPSSs) have been proved to be effective in realizing for strain management to prevent layer cracking. However, previous research showed that it is difficult to grow AlN directly on PSSs.^{25,26)} Recently, our group realized high-quality AlN/sapphire templates by combining sputtering and high-temperature annealing using a face-to-face method.²⁷⁾ Therefore, the application of a high-quality sputter-deposited annealed AlN film as the buffer layer instead of a nitrated NPSS for HVPE growth not only simplifies the growth process but may also improve the crystallinity owing to the high-quality AlN film on the *c*-plane region of the NPSS.

In this study, we aim to grow a high-quality thick AlN layer without cracks by HVPE on NPSS with a sputter-deposited annealed AlN film. The dependence of the crystallinity of AlN layers on the growth temperature was investigated. To the best of our knowledge, this is the first report of AlN growth on an NPSS with a sputter-deposited annealed AlN film by HVPE.

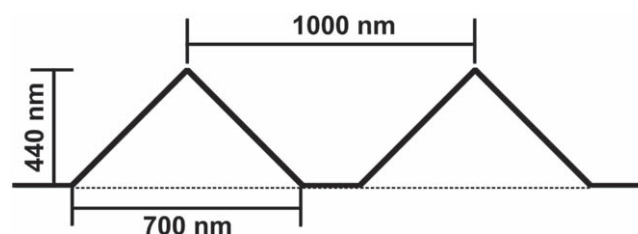


Fig. 1. Cross-sectional illustration of NPSS.

2. Experimental methods

A *c*-plane FSS and a commercially available *c*-plane-oriented NPSS were used in this study. The misorientation angle of the *c*-plane FSS and *c*-plane-oriented NPSS was 0.2° toward the [1–100] direction. The NPSS has a hexagonal arrangement of cone structures on the front side, as shown in Fig. 1. An AlN film of 200 nm thickness was deposited on sapphire by sputtering. Subsequently, the sputter-deposited AlN film was thermally annealed in N_2 at 1700°C for 3 h using the “face-to-face” setup.²⁷⁾ The template was used as a substrate for HVPE homo-epitaxial growth. Polycrystalline AlN was used as a target and the ambient was an argon (Ar) and nitrogen (N_2) gas mixture with the ratio $[\text{Ar}]/[\text{N}_2] = 0.25$. The radio-frequency (RF) power and growth temperature were 700 W and 600°C , respectively. The AlN layer was grown by HVPE using an RF heating system. The growth temperature and pressure were 1400°C – 1550°C and 10 kPa, respectively. The growth duration was 30 min. NH_3 , Al, and HCl were used as source materials, and N_2 and H_2 were used as carrier gases. The source of AlCl_3 was formed by the reaction of Al and HCl at 550°C in the source zone of the reactor, and AlCl_3 was then reacted with NH_3 in the growth zone, producing AlN layers. The flow rates of HCl and NH_3 were 40 and 50 sccm, respectively. The surface morphology and structure of the AlN layer were characterized by optical microscopy and scanning electron microscopy (SEM). The crystallinity of the AlN films was determined by XRD analysis using an asymmetric Ge(220) monochromator with

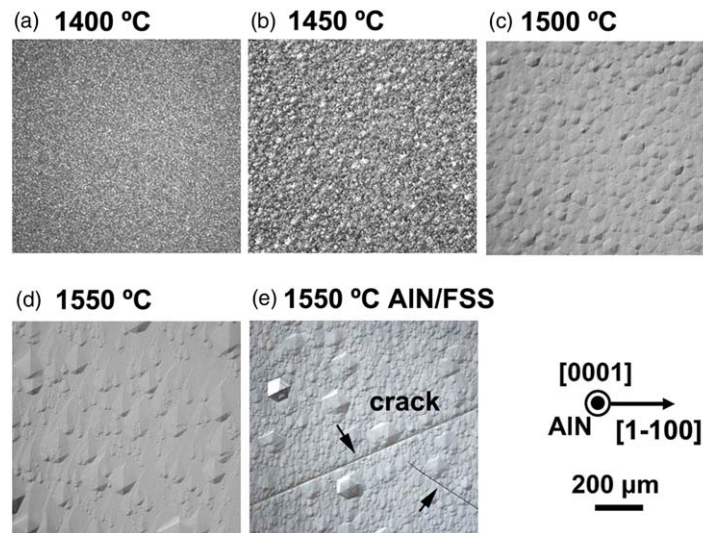


Fig. 2. (Color online) NorMarski images of AlN layers grown on NPSSs with sputter-deposited annealed AlN films at (a) 1400 °C, (b) 1450 °C, (c) 1500 °C, and (d) 1550 °C and AlN layer on (e) FSS at 1550 °C.

Cu K-alpha 1 radiation (wavelength, 0.154 nm) and Raman analysis. KOH etching was conducted at 80 °C for 5 min for polarity characterization. The molar concentration of KOH solution was 8 mol l⁻¹. Specimens for cross-sectional transmission electronic microscopy (TEM) observation along the [11-20] AlN direction were prepared using a focused ion beam.

3. Results and discussion

The cross-sectional SEM observation proved that the sputter-deposited annealed AlN films on the *c*-plane of NPSSs (regions between cone structures) were relatively smooth because of the solid-phase reaction during high-temperature annealing. On the other hand, the KOH etching confirmed that the grains with *c*-axis-oriented AlN were on the *c*-plane and cone tips of the NPSS. The results of SEM and KOH etching of sputter-deposited annealed AlN films will be published elsewhere. The FWHM values of symmetric (0002) and asymmetric (10-12) AlN X-ray Bragg diffraction peaks were too broad and weak to be measured for the sputter-deposited annealed AlN film on the NPSS, which resulted from the growth of the AlN film on non-*c*-plane sapphire facets (cone region) exhibiting several crystal orientations. Figures 2(a)–2(d) show the surface morphology of the HVPE-grown AlN layer at different growth temperatures on the NPSS with sputter-deposited annealed AlN films. The surface morphology of the AlN layer grown at 1550 °C on the FSS with sputter-deposited annealed AlN films is indicated in Fig. 2(e). The surfaces of the AlN layers grown at 1400 °C and 1450 °C were too rough to be observed by NorMarski microscopy, as respectively shown in Figs. 2(a) and 2(b). With increasing growth temperature above 1500 °C, hexagonal hillocks, which were commonly observed on the surface of HVPE-grown AlN layers, could be observed, as shown in Figs. 2(c) and 2(d).²⁸⁾ The hillocks on the surface of AlN grown at 1550 °C, as shown in Fig. 2(d), had relatively gentle sidewalls, as confirmed by SEM observation later. No pits were observed on the surface, indicating the complete coalescence of the AlN layer at growth temperatures above 1500 °C. The XRC shown in Fig. 3 indicated that

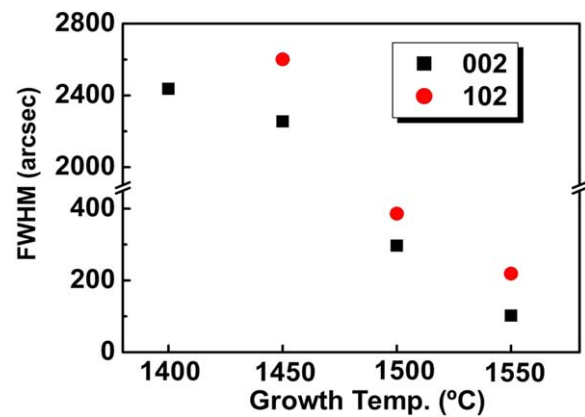


Fig. 3. (Color online) FWHMs of (0002)- and (10-12)-plane XRCs of AlN layers grown on NPSS with sputter-deposited annealed AlN films at 1400 °C–1550 °C.

the crystallinity of the AlN layers was improved with increasing growth temperature. The FWHM values of asymmetric (10-12) AlN X-ray Bragg diffraction peaks were too broad and weak to be measured for HVPE-grown AlN layer on NPSS with the sputter-deposited annealed AlN film at 1400 °C. The growth rate decreased with increasing temperature because the gas-phase transport was suppressed. The growth rates were approximately 24 and 20 μm h⁻¹ at 1400 °C and 1550 °C, respectively. When the growth temperature was increased to above 1550 °C, the growth rate decreased markedly because of the desorption of AlN. Thus, the growth conducted above 1550 °C was not considered in this study. The FWHM values of symmetric (0002) and asymmetric (10-12) AlN X-ray Bragg diffraction peaks decreased with increasing growth temperature and were improved to as low as 102 and 219 arcsec, respectively. On the other hand, the FWHM values of the (0002) and (10-12) peaks of AlN grown under the same conditions on an FSS with the sputter-deposited annealed AlN film were 70 and 395 arcsec, respectively. Note that the 9 ± 1 μm thick AlN layer grown on the NPSS with the sputter-deposited annealed AlN film was crack-free, whereas cracks were observed on

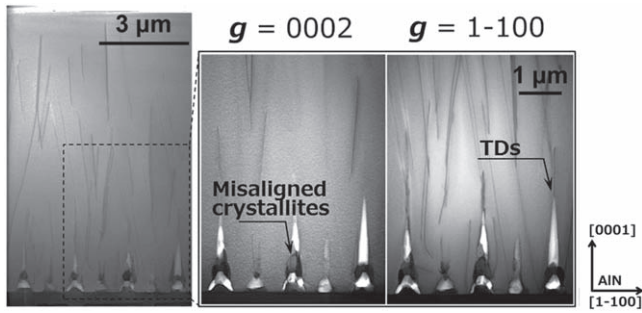


Fig. 6. Cross-sectional TEM images of AlN layers grown on NPSS with sputter-deposited annealed AlN film at 1550 °C. Two-beam diffraction conditions were used to identify the line dislocations near the AlN/sapphire interface.

On the basis of the SEM observations, the growth processes at 1400 °C and 1550 °C are respectively illustrated in Figs. 5(a) and 5(b). The growth rates at 1400 °C were almost the same in the non-*c*-plane and the *c*-plane surface of the NPSS because the migration of Al species was relatively slower than that at 1550 °C. The Al species were uniformly distributed in both non-*c*-plane and *c*-plane surface of the NPSS, which resulted in almost the same growth rates of AlN in both regions at 1400 °C. Since the *c*-axis-oriented growth on the *c*-plane could not continue owing to the blocking of AlN growth by misaligned AlN crystallites in the non-*c*-plane region, the crystallinity of the AlN layer deteriorated. When the growth temperature increased to 1550 °C, the migration of Al species was promoted primarily forward to the *c*-axis surface, which was energy-stable. The *c*-axis-oriented growth rate of AlN in the *c*-plane region of the NPSS was much higher than that on the non-*c*-axis plane, which led to the improvement of AlN crystallinity. Moreover, the high-quality sputter-deposited annealed AlN film in the *c*-plane region of the NPSS was also assumed to contribute to the high crystallinity during homoepitaxy. The formation of various facets on the AlN layer surface at different growth temperatures could be explained by the equilibrium crystal shape theory, which indicates that the surface energies of the crystal plane vary with the growth temperature.^{36–38} The facet of the growth front on the surface is the *c*-axis plane since its free energy is lowest when the growth temperature is sufficiently high. The stable facet is expected to change to non-*c*-axis facets when the growth temperature is, in our case, lower than 1450 °C. It was proved that when the growth temperature is sufficiently high, AlN growth is along the [0001] direction and (0001) is the facet on the surface.

Cross-sectional TEM was conducted to investigate the dislocation behaviors in the HVPE-grown AlN layer on the NPSS with a sputter-deposited annealed AlN film, as shown in Fig. 6. It is found that the AlN layer completely coalesced and had coalescence thickness of about 1.8 μm, which was less than the previously reported coalescence thicknesses for AlN grown on micropatterned substrates using ELO technique.³⁹ Black contrast areas indicate misaligned crystallites located on the non-*c*-axis sapphire plane, which was consistent with our hypothesis based on the SEM observation mentioned above, as shown in Fig. 5(b). Two-beam diffraction conditions were used to characterize the dislocations near the interface between the AlN and NPSS. As shown in Fig. 6, it is evident that threading dislocations are mainly

generated at the coalescence boundary instead of the *c*-axis-oriented sapphire plane. The TEM observation proved that the high-quality sputter-deposited annealed AlN film in the *c*-plane region of the NPSS contributes to the high crystallinity during homoepitaxy. Moreover, the results show that it is crucial to control the lateral growth rate since a high growth rate in the lateral direction results in tilted growth fronts. An increase in the lateral growth rate should lead to worsening of disorientations among different coalescence regions above the voids.

4. Conclusions

AlN were grown on NPSSs and FSSs with sputter-deposited annealed AlN films by HVPE and the HVPE-grown AlN layers were characterized. The crystallinity of AlN layers grown on the NPSSs with sputter-deposited annealed AlN films improved with increasing growth temperature. A higher temperature for HVPE growth was found to promote the formation of *c*-oriented AlN layers and suppress the formation of disoriented crystallites on the non-*c*-axis planes, resulting in the improved crystallinity. Moreover, 9 ± 1 μm thick AlN layers without cracks were fabricated on the NPSSs with sputter-deposited annealed AlN films at 1550 °C and the FWHMs of the (0002)- and (10–12)-plane X-ray rocking curves were improved to as low as 102 and 219 arcsec, respectively. The NPSSs with sputter-deposited annealed AlN films are promising for realizing high-quality and large-scale freestanding AlN substrates or templates without cracks by HVPE growth.

Acknowledgments

This work was partially supported by “Program for Building Regional Innovation Ecosystems”, “Program for Research and Development of Next-generation Semiconductor to Realize Energy-saving Society”, MEXT, JSPS KAKENHI Grants (JP16H06415), JST CREST (16815710), JST SICORP EU H2020 No. 720527 (InRel-NPower) and JST SICORP with MOST in China.

- 1) A. Fujioka, T. Misaki, T. Murayama, Y. Narukawa, and T. Mukai, *Appl. Phys. Express* **3**, 041001 (2010).
- 2) K. Ban, J. Yamamoto, K. Takeda, K. Ide, M. Iwaya, T. Takeuchi, S. Kamiyama, I. Akasaki, and H. Amano, *Appl. Phys. Express* **4**, 052101 (2011).
- 3) H. Hirayama, *J. Appl. Phys.* **97**, 091101 (2005).
- 4) R. T. Bondokov, S. G. Mueller, K. E. Morgan, G. A. Slack, S. Schujman, M. C. Wood, J. A. Smart, and L. J. Schowalter, *J. Cryst. Growth* **310**, 4020 (2008).
- 5) C. Hartmann, J. Wollweber, A. Dittmar, K. Irmischer, A. Kwasniewski, F. Langhans, T. Neugut, and M. Bickermann, *J. Appl. Phys.* **52**, 08JA06 (2013).
- 6) H. Hirayama, S. Fujikawa, N. Noguchi, J. Norimatsu, T. Takano, K. Tsubaki, and N. Kamata, *Phys. Status Solidi A* **206**, 1176 (2009).
- 7) Y. Taniyasu, M. Kasu, and T. Makimoto, *Nature* **441**, 325 (2006).
- 8) Y. Shimahara, H. Miyake, K. Hiramatsu, F. Fukuyo, T. Okada, H. Takaoka, and H. Yoshida, *Appl. Phys. Express* **4**, 042103 (2011).
- 9) Y. Taniyasu, M. Kasu, and N. Kobayashi, *Appl. Phys. Lett.* **81**, 1255 (2002).
- 10) A. Khan, K. Balakrishnan, and T. Katona, *Nat. Photonics* **2**, 77 (2008).
- 11) C. Hartmann, J. Wollweber, S. Sintonen, A. Dittmar, L. Kirste, S. Kollowa, K. Irmischer, and M. Bickermann, *Cryst. Eng. Commun.* **18**, 3488 (2016).
- 12) T. Nagashima, Y. Kubota, T. Kinoshita, Y. Kumagai, J. Xie, R. Collazo, H. Murakami, H. Okamoto, A. Koukitu, and Z. Sitar, *Appl. Phys. Express* **5**, 125501 (2012).
- 13) Y. Kumagai et al., *Appl. Phys. Express* **5**, 055504 (2012).
- 14) P. Wu, M. Funato, and Y. Kawakami, *Sci. Rep.* **5**, 17405 (2015).

- 15) B. Tran, H. Hirayama, N. Maeda, M. Jo, S. Toyada, and N. Kamata, *Sci. Rep.* **5**, 14734 (2015).
- 16) D. Zhang, F. Liu, and L. Cai, *Phys. Status Solidi A* **211**, 2394 (2014).
- 17) J. Tajima, Y. Kubota, R. Togashi, H. Murakami, Y. Kumagai, and A. Koukitu, *Phys. Status Solidi C* **5**, 1515 (2008).
- 18) Y. Kumagai, T. Nagashima, and A. Koukitu, *Jpn. J. Appl. Phys.* **46**, L389 (2007).
- 19) T. Nagashima, M. Harada, H. Yanagi, Y. Kumagai, A. Koukitu, and K. Takada, *J. Cryst. Growth* **300**, 42 (2007).
- 20) O. Kovalenkov, V. Soukhovuev, V. Ivantsov, A. Usikov, and V. Dmitriev, *J. Cryst. Growth* **281**, 87 (2005).
- 21) K. Tsujisawa, S. Kishino, D. B. Li, H. Miyake, K. Hiramatsu, T. Shibata, and M. Tanaka, *Jpn. J. Appl. Phys.* **46**, L552 (2007).
- 22) D. S. Kamber, Y. Wu, B. A. Haskell, S. Newman, S. P. DenBaars, J. S. Speck, and S. Nakamura, *J. Cryst. Growth* **297**, 321 (2006).
- 23) J. Tajima, R. Togashi, H. Murakami, Y. Kumagai, K. Takada, and A. Koukitu, *Phys. Status Solidi C* **8**, 2028 (2011).
- 24) V. Soukhovuev, A. Volkova, V. Ivantsov, O. Kovalenkov, A. Syркиn, and A. Usikov, *Phys. Status Solidi C* **6**, S333 (2009).
- 25) H. Hirayama, Y. Tomita, S. Toyada, S. Fujikawa, and N. Kamata, Proc. Conf. Lasers and Electro-Optics Pacific Rim, 2013, W H2-2.
- 26) L. X. Zhao, Z. G. Yu, B. Sun, S. C. Zhu, P. B. An, C. Yang, L. Liu, J. X. Wang, and J. M. Li, *Chin. Phys. B* **24**, 068506 (2015).
- 27) H. Miyake, C. H. Lin, K. Tokoro, and K. Hiramatsu, *J. Cryst. Growth* **456**, 155 (2016).
- 28) T. Baker, A. Mayo, Z. Veisi, P. Lu, and J. Schmitt, *Phys. Status Solidi C* **11**, 373 (2014).
- 29) Y. Kida, T. Shibata, H. Naoi, H. Miyake, K. Hiramatsu, and M. Tanaka, *Phys. Status Solidi A* **194**, 498 (2002).
- 30) M. Pons, J. Su, M. Chubarov, R. Boichot, F. Mercier, E. Blanquet, G. Giusti, and D. Pique, *J. Cryst. Growth* **486**, 235 (2017).
- 31) M. D. Thouless, Z. Li, N. J. Douville, and S. Takayama, *J. Mech. Phys. Solids* **59**, 1927 (2011).
- 32) M. Kuball, *Surf. Interface Anal.* **31**, 987 (2001).
- 33) S. Hagedorn, A. Knauer, A. Mogilatenko, E. Richter, and M. Weyers, *Phys. Status Solidi A* **213**, 3178 (2016).
- 34) J. A. Freitas Jr., J. C. Culbertson, M. A. Mastro, Y. Kumagai, and A. Koukitu, *J. Cryst. Growth* **350**, 33 (2012).
- 35) Y. Kumagai, T. Ii, M. Ishizuki, R. Togashi, H. Murakami, K. Takada, and A. Koukitu, *J. Cryst. Growth* **350**, 60 (2012).
- 36) N. Moll, A. Kley, E. Pehlke, and M. Scheffler, *Phys. Rev. B* **54**, 8844 (1996).
- 37) C. Rottman and M. Wortis, *Phys. Rep.* **103**, 59 (1984).
- 38) T. Liu, J. Zhang, X. Su, J. Huang, J. Wang, and K. Xu, *Sci. Rep.* **6**, 26040 (2016).
- 39) Y. Watanabe, H. Miyake, K. Hiramatsu, Y. Iwasaki, and S. Nagata, *Phys. Status Solidi C* **12**, 334 (2015).